First measurement of the ν_μ charged-current cross section on a water target without pions in the final state

K. Abe,[45] J. Amey,[15] C. Andreopoulos,[43,25] M. Antonova,[20] S. Aoki,[22] A. Ariga,[1] Y. Ashida,[23] S. Ban,[23] M. Barbi,[37] G. J. Barker,[53] G. Barr,[33] C. Barry,[25] M. Batkiewicz,[11] V. Berardi,[16] S. Berkman,[3,49] S. Bhadra,[57] S. Bienstock,[34] A. Blondel,[10] S. Bolognesi,[5] S. Bordoni,[13,*] S. B. Boyd,[53] D. Brailsford,[24] A. Bravar,[10] C. Bronner,[45] M. Buizza Avanzini,[9] R. G. Calland,[21] T. Campbell,[7] S. Cao,[12] S. L. Cartwright,[41] M. G. Catanesi,[16] A. Cervera,[14] A. Chappell,[53] C. Checchia,[18] D. Cherdack,[7] N. Chikuma,[44] G. Christodoulou,[25] J. Coleman,[25] G. Collazuol,[18] D. Coplowe,[33] A. Cudd,[27] A. Dabrowska,[11] G. De Rosa,[17] T. Dealtry,[24] P. F. Denner,[53] S. R. Dennis,[25] C. Densham,[43] F. Di Lodovico,[36] S. Dolan,[33] O. Drapier,[9] K. E. Duffy,[33] J. Dumarchez,[34] P. Dunne,[15] S. Emery-Schrenk,[5] A. Ereditato,[1] T. Feusels,[3,49] A. J. Finch,[24] G. A. Fiorentini,[57] M. Friend,[12,†] Y. Fujii,[12,†] D. Fukuda,[31] Y. Fukuda,[28] A. Garcia,[13] C. Giganti,[34] F. Gizzarelli,[5] T. Golan,[55] M. Gonin,[9] D. R. Hadley,[53] L. Haegel,[10] J. T. Haigh,[53] D. Hansen,[35] J. Harada,[32] M. Hartz,[21,49] T. Hasegawa,[12,†] N. C. Hastings,[37] T. Hayashino,[23] Y. Hayato,[45,21] A. Hillairet,[50] T. Hiraki,[23] A. Hiramoto,[23] S. Hirota,[23] M. Hogan,[7] J. Holeczek,[42] F. Hosomi,[44] K. Huang,[23] A. K. Ichikawa,[23] M. Ikeda,[45] J. Imber,[9] J. Insler,[26] R. A. Intonti,[16] T. Ishida,[12,†] T. Ishii,[12,†] E. Iwai,[12] K. Iwamoto,[44] A. Izmaylov,[14,20] B. Jamieson,[54] M. Jiang,[23] S. Johnson,[6] P. Jonsson,[15] C. K. Jung,[30,‡] M. Kabirnezhad,[29] A. C. Kaboth,[39,43] T. Kajita,[46,‡] H. Kakuno,[47] J. Kameda,[45] D. Karlen,[50,49] T. Katori,[36] E. Kearns,[2,21,‡] M. Khabibullin,[20] A. Khotjantsev,[20] H. Kim,[32] J. Kim,[3,49] S. King,[36] J. Kisiel,[42] A. Knight,[53] A. Knox,[24] T. Kobayashi,[12,†] L. Koch,[40] T. Koga,[44] P. P. Koller,[1] A. Konaka,[49] L. L. Kormos,[24] Y. Koshio,[31,‡] K. Kowalik,[29] Y. Kudenko,[20,§] R. Kurjata,[52] T. Kutter,[26] J. Lagoda,[29] I. Lamont,[24] M. Lamoureux,[5] P. Lasorak,[36] M. Laveder,[18] M. Lawe,[24] M. Licciardi,[9] T. Lindner,[49] Z. J. Liptak,[6] R. P. Litchfield,[15] X. Li,[30] A. Longhin,[18] J. P. Lopez,[6] T. Lou,[44] L. Ludovici,[19] X. Lu,[33] L. Magaletti,[16] K. Mahn,[27] M. Malek,[41] S. Manly,[38] L. Maret,[10] A. D. Marino,[6] J. F. Martin,[48] P. Martins,[36] S. Martynenko,[30] T. Maruyama,[12,†] V. Matveev,[20] K. Mavrokoridis,[25] W. Y. Ma,[15] E. Mazzucato,[5] M. McCarthy,[57] N. McCauley,[25] K. S. McFarland,[38] C. McGrew,[30] A. Mefodiev,[20] C. Metelko,[25] M. Mezzetto,[18] A. Minamino,[56] O. Mineev,[20] S. Mine,[4] A. Missert,[6] M. Miura,[45,‡] S. Moriyama,[45,‡] J. Morrison,[27] Th. A. Mueller,[9] T. Nakadaira,[12,†] M. Nakahata,[45,21] K. G. Nakamura,[23] K. Nakamura,[21,12,†] K. D. Nakamura,[23] Y. Nakanishi,[23] S. Nakayama,[45,‡] T. Nakaya,[23,21] K. Nakayoshi,[12,†] C. Nantais,[48] C. Nielsen,[3,49] K. Nishikawa,[12,†] Y. Nishimura,[46] P. Novella,[14] J. Nowak,[24] H. M. O'Keeffe,[24] K. Okumura,[46,21] T. Okusawa,[32] W. Oryszczak,[51] S. M. Oser,[3,49] T. Ovsyannikova,[20] R. A. Owen,[36] Y. Oyama,[12,†] V. Palladino,[17] J. L. Palomino,[30] V. Paolone,[35] N. D. Patel,[23] P. Paudyal,[25] M. Pavin,[34] D. Payne,[25] Y. Petrov,[3,49] L. Pickering,[15] E. S. Pinzon Guerra,[57] C. Pistillo,[1] B. Popov,[34,‖] M. Posiadala-Zezula,[51] J.-M. Poutissou,[49] A. Pritchard,[25] P. Przewlocki,[29] B. Quilain,[23] T. Radermacher,[40] E. Radicioni,[16] P. N. Ratoff,[24] M. A. Rayner,[10] E. Reinherz-Aronis,[7] C. Riccio,[17] E. Rondio,[29] B. Rossi,[17] S. Roth,[40] A. C. Ruggeri,[17] A. Rychter,[52] K. Sakashita,[12,†] F. Sánchez,[13] E. Scantamburlo,[10] K. Scholberg,[8,‡] J. Schwehr,[7] M. Scott,[49] Y. Seiya,[32] T. Sekiguchi,[12,†] H. Sekiya,[45,21,‡] D. Sgalaberna,[10] R. Shah,[43,33] A. Shaikhiev,[20] F. Shaker,[54] D. Shaw,[24] M. Shiozawa,[45,21] T. Shirahige,[31] M. Smy,[4] J. T. Sobczyk,[55] H. Sobel,[4,21] J. Steinmann,[40] T. Stewart,[43] P. Stowell,[41] Y. Suda,[44] S. Suvorov,[20] A. Suzuki,[22] S. Y. Suzuki,[12,†] Y. Suzuki,[21] R. Tacik,[37,49] M. Tada,[12,†] A. Takeda,[45] Y. Takeuchi,[22,21] R. Tamura,[44] H. K. Tanaka,[45,‡] H. A. Tanaka,[48,49,¶] T. Thakore,[26] L. F. Thompson,[41] S. Tobayama,[3,49] W. Toki,[7] T. Tomura,[45] T. Tsukamoto,[12,†] M. Tzanov,[26] M. Vagins,[21,4] Z. Vallari,[30] G. Vasseur,[5] C. Vilela,[30] T. Vladisavljevic,[33,21] T. Wachala,[11] C. W. Walter,[8,‡] D. Wark,[43,33] M. O. Wascko,[15] A. Weber,[43,33] R. Wendell,[23,‡] M. J. Wilking,[30] C. Wilkinson,[1] J. R. Wilson,[36] R. J. Wilson,[7] C. Wret,[15] Y. Yamada,[12,†] K. Yamamoto,[32] C. Yanagisawa,[30,**] T. Yano,[22] S. Yen,[49] N. Yershov,[20] M. Yokoyama,[44,‡] T. Yuan,[6] M. Yu,[57] A. Zalewska,[11] J. Zalipska,[29] L. Zambelli,[12,†] K. Zaremba,[52] M. Ziembicki,[52] E. D. Zimmerman,[6] and M. Zito[5]

(T2K Collaboration)

[1]*University of Bern, Albert Einstein Center for Fundamental Physics, Laboratory for High Energy Physics (LHEP), Bern, Switzerland*
[2]*Boston University, Department of Physics, Boston, Massachusetts, USA*
[3]*University of British Columbia, Department of Physics and Astronomy, Vancouver, British Columbia, Canada*
[4]*University of California, Irvine, Department of Physics and Astronomy, Irvine, California, USA*
[5]*IRFU, CEA Saclay, Gif-sur-Yvette, France*
[6]*University of Colorado at Boulder, Department of Physics, Boulder, Colorado, USA*
[7]*Colorado State University, Department of Physics, Fort Collins, Colorado, USA*
[8]*Duke University, Department of Physics, Durham, North Carolina, USA*

[9]*Ecole Polytechnique, IN2P3-CNRS, Laboratoire Leprince-Ringuet, Palaiseau, France*
[10]*University of Geneva, Section de Physique, DPNC, Geneva, Switzerland*
[11]*H. Niewodniczanski Institute of Nuclear Physics PAN, Cracow, Poland*
[12]*High Energy Accelerator Research Organization (KEK), Tsukuba, Ibaraki, Japan*
[13]*Institut de Fisica d'Altes Energies (IFAE), The Barcelona Institute of Science and Technology, Campus UAB, Bellaterra (Barcelona) Spain*
[14]*IFIC (CSIC & University of Valencia), Valencia, Spain*
[15]*Imperial College London, Department of Physics, London, United Kingdom*
[16]*INFN Sezione di Bari and Università e Politecnico di Bari, Dipartimento Interuniversitario di Fisica, Bari, Italy*
[17]*INFN Sezione di Napoli and Università di Napoli, Dipartimento di Fisica, Napoli, Italy*
[18]*INFN Sezione di Padova and Università di Padova, Dipartimento di Fisica, Padova, Italy*
[19]*INFN Sezione di Roma and Università di Roma "La Sapienza", Roma, Italy*
[20]*Institute for Nuclear Research of the Russian Academy of Sciences, Moscow, Russia*
[21]*Kavli Institute for the Physics and Mathematics of the Universe (WPI), The University of Tokyo Institutes for Advanced Study, University of Tokyo, Kashiwa, Chiba, Japan*
[22]*Kobe University, Kobe, Japan*
[23]*Kyoto University, Department of Physics, Kyoto, Japan*
[24]*Lancaster University, Physics Department, Lancaster, United Kingdom*
[25]*University of Liverpool, Department of Physics, Liverpool, United Kingdom*
[26]*Louisiana State University, Department of Physics and Astronomy, Baton Rouge, Louisiana, USA*
[27]*Michigan State University, Department of Physics and Astronomy, East Lansing, Michigan, USA*
[28]*Miyagi University of Education, Department of Physics, Sendai, Japan*
[29]*National Centre for Nuclear Research, Warsaw, Poland*
[30]*State University of New York at Stony Brook, Department of Physics and Astronomy, Stony Brook, New York, USA*
[31]*Okayama University, Department of Physics, Okayama, Japan*
[32]*Osaka City University, Department of Physics, Osaka, Japan*
[33]*Oxford University, Department of Physics, Oxford, United Kingdom*
[34]*UPMC, Université Paris Diderot, CNRS/IN2P3, Laboratoire de Physique Nucléaire et de Hautes Energies (LPNHE), Paris, France*
[35]*University of Pittsburgh, Department of Physics and Astronomy, Pittsburgh, Pennsylvania, USA*
[36]*Queen Mary University of London, School of Physics and Astronomy, London, United Kingdom*
[37]*University of Regina, Department of Physics, Regina, Saskatchewan, Canada*
[38]*University of Rochester, Department of Physics and Astronomy, Rochester, New York, USA*
[39]*Royal Holloway University of London, Department of Physics, Egham, Surrey, United Kingdom*
[40]*RWTH Aachen University, III. Physikalisches Institut, Aachen, Germany*
[41]*University of Sheffield, Department of Physics and Astronomy, Sheffield, United Kingdom*
[42]*University of Silesia, Institute of Physics, Katowice, Poland*
[43]*STFC, Rutherford Appleton Laboratory, Harwell Oxford, and Daresbury Laboratory, Warrington, United Kingdom*
[44]*University of Tokyo, Department of Physics, Tokyo, Japan*
[45]*University of Tokyo, Institute for Cosmic Ray Research, Kamioka Observatory, Kamioka, Japan*
[46]*University of Tokyo, Institute for Cosmic Ray Research, Research Center for Cosmic Neutrinos, Kashiwa, Japan*
[47]*Tokyo Metropolitan University, Department of Physics, Tokyo, Japan*
[48]*University of Toronto, Department of Physics, Toronto, Ontario, Canada*
[49]*TRIUMF, Vancouver, British Columbia, Canada*
[50]*University of Victoria, Department of Physics and Astronomy, Victoria, British Columbia, Canada*
[51]*University of Warsaw, Faculty of Physics, Warsaw, Poland*
[52]*Warsaw University of Technology, Institute of Radioelectronics, Warsaw, Poland*

[53]University of Warwick, Department of Physics, Coventry, United Kingdom
[54]University of Winnipeg, Department of Physics, Winnipeg, Manitoba, Canada
[55]Wroclaw University, Faculty of Physics and Astronomy, Wroclaw, Poland
[56]Yokohama National University, Faculty of Engineering, Yokohama, Japan
[57]York University, Department of Physics and Astronomy, Toronto, Ontario, Canada

(Received 24 August 2017; published 8 January 2018)

This paper reports the first differential measurement of the charged-current interaction cross section of ν_μ on water with no pions in the final state. This flux-averaged measurement has been made using the T2K experiment's off-axis near detector, and is reported in doubly differential bins of muon momentum and angle. The flux-averaged total cross section in a restricted region of phase space was found to be $\sigma = (0.95 \pm 0.08(\text{stat}) \pm 0.06(\text{det syst}) \pm 0.04(\text{model syst}) \pm 0.08(\text{flux})) \times 10^{-38}$ cm^2/n.

DOI: 10.1103/PhysRevD.97.012001

I. INTRODUCTION

The Tokai-to-Kamioka (T2K) experiment [1] is a long-baseline neutrino oscillation experiment, with a beam originating at Japan Proton Accelerator Complex (J-PARC) which consists primarily of muon neutrinos. T2K has measured the disappearance of muon neutrinos [2] and the appearance of electron neutrinos [3], using the off-axis ND280 near detector on the J-PARC site, and the Super-Kamiokande detector [4], located 295 km away.

At the energies of the T2K beam line, the main neutrino interaction process is charged-current quasielastic (CCQE) interactions ($\nu_\mu + n \to \mu^- + p$). Because these neutrino interactions occur within nuclear targets and not on free nuclei, additional nuclear effects and final state interactions can modify the composition and kinematics of the particles that are observed to be exiting the interaction. This paper focuses on a measurement of CCQE-like events (in bins of the muon angle and momentum) in which no pions (charged or neutral) are observed in the final state (CC0π).

The active target regions of the ND280 near detector, as will be discussed in Sec. II, are primarily composed of plastic scintillator, but the far detector is water based. While the near detector measurements on hydrocarbon targets can help to greatly constrain the flux and cross section uncertainties for the oscillation analyses, one of the dominant remaining uncertainties is due to potential differences between the oxygen and carbon cross sections that are not currently well constrained by the ND280 detector [5]. The ND280 detector also contains water targets, and this paper presents a measurement of the ν_μ CC0π interaction cross section on water. This process is very important for T2K's neutrino oscillation measurements since this is the dominant reaction in the far detector.

While there are differential measurements of the CCQE cross sections on carbon or hydrocarbon [6–10], there are none on water. The K2K experiment has published a measurement of the axial vector mass in neutrino-oxygen CCQE interactions [11] using the SciFi detector, but not a differential cross section measurement.

II. THE T2K EXPERIMENT

A high-intensity beam is produced at J-PARC at Tokai village, Ibaraki, Japan and directed to Super-Kamiokande. In order to enhance the sensitivity to T2K's primary physics goals, the appearance of electron neutrinos and the disappearance of muon neutrinos, the beam energy peaks at the oscillation maximum of 0.6 GeV, and this is achieved by adopting the off-axis method [1].

A. The T2K beam line

High-intensity 30 GeV protons from the J-PARC accelerator strike a graphite target every 2.48 seconds and produce charged pions and kaons. These pions and kaons are focused to the forward direction by three horn magnets [12] and decay in the 96-m long decay volume. Neutrinos (antineutrinos) are produced from decays of positively (negatively) charged pions. Horn magnets select pions of either sign by flipping the current direction.

T2K started data taking in 2010 with a beam of primarily muon neutrinos until May 2014 and then started data taking with a primarily muon antineutrino beam until May 2016, and is continuing to take data. The analysis presented here uses data taken in the neutrino mode.

*Now at CERN.
†Also at J-PARC, Tokai, Japan.
‡Also at Kavli IPMU (WPI), the University of Tokyo, Japan.
§Also at National Research Nuclear University "MEPhI" and Moscow Institute of Physics and Technology, Moscow, Russia.
‖Also at JINR, Dubna, Russia.
¶Also at Institute of Particle Physics, Canada.
**Also at BMCC/CUNY, Science Department, New York, New York, USA.

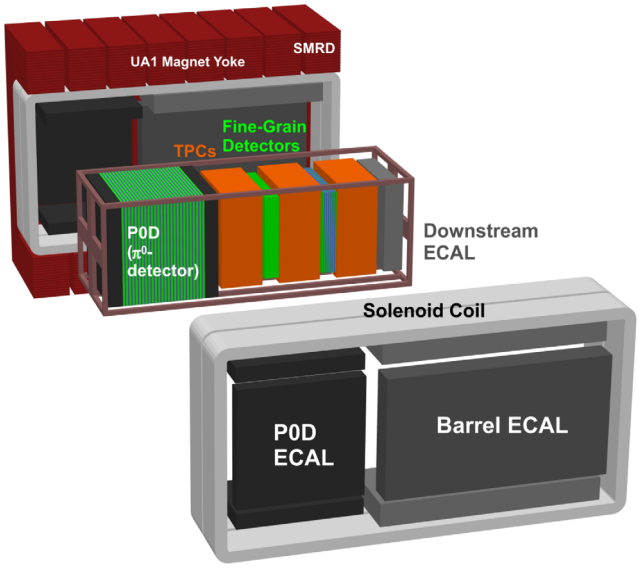

FIG. 1. An exploded view of T2K's off-axis near detector.

The neutrino flux is calculated based on the measurement of primary proton beam profiles and hadron production data, including the measurement of the pion and kaon yields [13] by the NA61/SHINE experiment [14] at CERN. The total absolute flux uncertainty is about 10% at the peak energy, and details of the flux calculation are described in Ref. [15].

B. The T2K ND280 near detector

This analysis looks for neutrino interactions in the T2K off-axis near detector, shown in Fig. 1, specifically for events in the pi-zero (PØD) subdetector. This subdetector, described in more detail in [16], consists of alternating planes of scintillator bars, sandwiched between lead or brass radiator layers. A more detailed schematic of the PØD is shown in Fig. 2. There are a total of 40 scintillator modules in the PØD, each one composed of a vertical layer of triangular scintillator bars and a layer of horizontal bars. In the upstream and downstream portions of the PØD (the "upstream ECal" and the "central ECal"), the scintillator layers alternate with lead sheets. The central 25 layers alternate the scintillator layers with brass sheets and bladders which can be filled with water or air. This analysis will use data taken in both configurations. The total mass of water in the PØD in the fiducial volume is approximately 1902 kg. Downstream of the PØD is a tracker with three TPCs [17] and two fine-grained scintillator detectors [18]. The PØD and tracker are surrounded by electromagnetic calorimeters [19] inside a magnet with a 0.2 T field that is instrumented with muon detectors [20].

III. ANALYSIS

A. Event selection

Hadrons produced within the nucleus are subject to final state interactions (FSIs) that can reabsorb the hadron or alter their kinematics as they emerge from the nucleus. Pion absorption for example can make a charged-current resonant (CCRES) interaction appear as a CCQE final state. This forces the selection to be based on a topology classified by the number and type of outgoing particles from the nucleus in order to be less model dependent. A single muon and zero pion topology is called CCQE-like or CC0π. The event selection identifies CC0π-enhanced samples by selecting events where a single track was reconstructed in the PØD. Identical selections are applied to both the water-in and water-out samples.

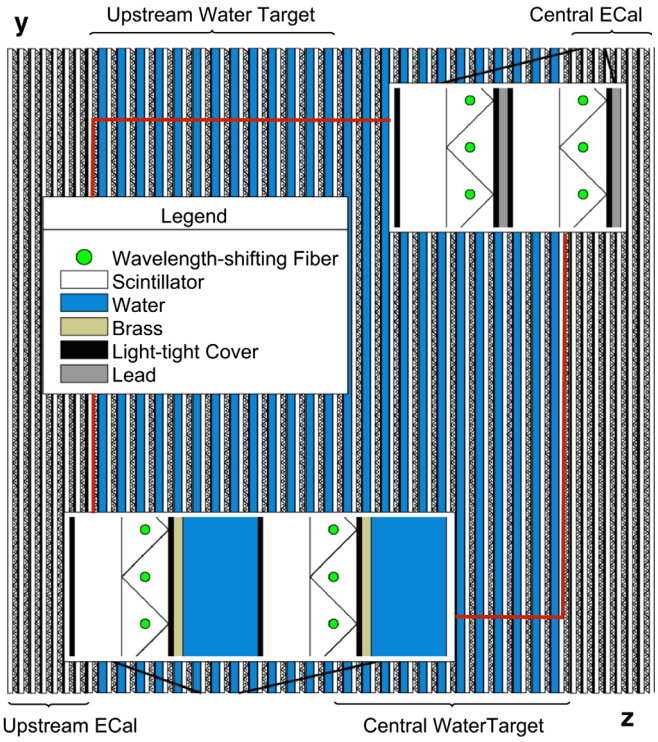

FIG. 2. A schematic of the PØD, showing the structure of the layers. The beam travels from the left to the right. The red box outlines the approximate fiducial volume used for this analysis.

The result in this paper relies on a subset of the neutrino mode data as broken down in Table I and totaling 5.52×10^{20} protons on the target (POT). The selection starts by identifying beam spills where the spill information and all ND280 subdetectors are known to have high-quality data. Each spill of the proton beam consists of several

TABLE I. T2K runs and their associated POT, filtered for spills where all ND280 detectors were flagged with good data quality.

T2K Run	POT
2 Water	4.29×10^{19}
2 Air	3.55×10^{19}
3c Air	1.35×10^{20}
4 Water	1.63×10^{20}
4 Air	1.76×10^{20}
Total	5.52×10^{20}

clearly separated bunches of protons. The selection then selects bunches containing tracks reconstructed in the TPCs associated with vertices reconstructed within the PØD fiducial volume, which extends from the middle of the scintillator of the first water layer to the middle of the scintillator in the last water layer and 25 cm in from the edges in the xy-plane (Fig. 2). In practice, these tracks are reconstructed from segments found in the PØD and TPC subdetector reconstruction processes. After identifying these bunches, the analysis identifies the highest-momentum negatively charged track as the muon candidate. If no negatively charged track is found, the bunch is removed from the selection. The selection then applies a TPC quality cut, removing tracks with no more than 18 nodes in the TPC reconstruction. The final cut for the selected CC0π sample requires that only a single track was reconstructed anywhere in the PØD in that bunch. The cross section reported here is restricted to bins in the region of muon kinematics where $\cos\theta_\mu \geq 0$ and $p_\mu \leq 5$ GeV. The total number of selected events in the water-in data sample is 12 777 (and based on simulations it is expected that approximately 3860 of these events are true interactions on water) and the total number in the water-out data (which has a larger POT exposure) sample is 13 370. Due to the requirement of a negatively charged track, the $\bar{\nu}_\mu$ contamination is this sample is very small and is estimated to be approximately 0.1% for both samples.

Figure 3 shows distributions of events that pass the selection for the water-in sample for data and a Monte Carlo (MC) detector simulation. The MC simulation chain primarily uses the NEUT neutrino event generator [21] to provide the kinematics for particles emerging from neutrino interactions and a GEANT4-based [22,23] package to simulate these particles moving through the detector (using GEANT version 4.9.4). The QGSP_BERT model is used for hadronic interactions. The MC distribution is separated by interaction channel. A detailed review of neutrino interactions can be found in [24] for example. The two largest sources of background are charged-current interactions with a single outgoing π^+ (CC1π^+) and any other charged-current interaction (CCOther) not categorized as CC0π or CC1π^+. The CC1π^+ topology is due primarily to pion resonance production and CCOther to deep inelastic scattering [24]. Additionally, neutral current backgrounds are classified as "BKG" and interactions occurring outside the PØD fiducial volume are classified as "out of FV" or "OOFV." Distributions for the water-out sample look similar.

To provide a data-driven constraint on the background, sideband selections are used for the CC1π^+ and CCOther topologies. Their selection is identical to the signal selection with the exception of the final cut. For the CC1π^+ sideband, events with exactly two PØD reconstructed tracks in a bunch along with at least one PØD reconstructed Michel electron are selected. For the CCOther sideband, events with greater than two PØD reconstructed tracks are selected. These cuts reduce overlap between the signal and sideband selections as shown in Figs. 4 and 5 for the water-in samples. The water-out sideband samples look very similar. The numbers of selected events in the signal and sidebands regions are summarized in Tables II and III.

B. Cross section extraction

The event selections described above are binned in the reconstructed double differential $(p_\mu, \cos\theta_\mu)$ phase space. Reconstructed kinematics are approximations to the true initial state of the muon. To extract the true kinematics from the reconstructed, an unfolding technique is used based

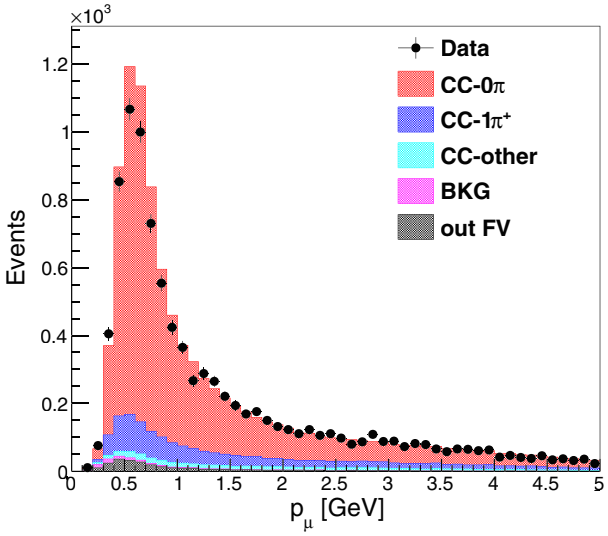

FIG. 3. Data and MC distributions of the water-in CC0π signal selection. NEUT 5.3.2 MC has been normalized to data POT and is sorted into various truth topologies.

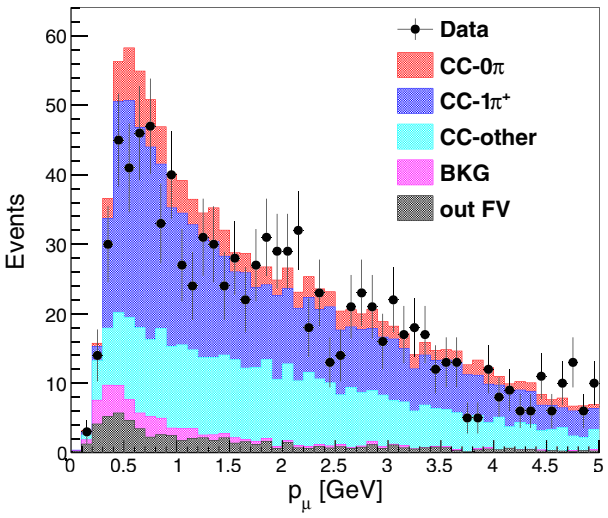

FIG. 4. Data and MC distributions of the water-in CC1π^+ sideband selection. NEUT 5.3.2 MC has been normalized to data POT and is sorted into various truth topologies.

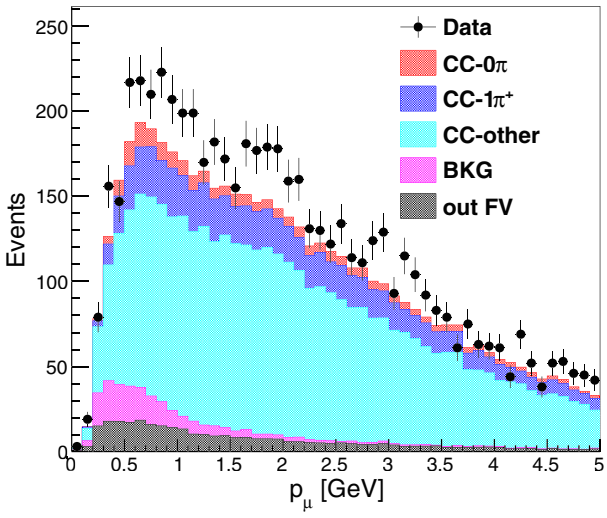

FIG. 5. Data and MC distributions of the water-in CCOther sideband selection. NEUT 5.3.2 MC has been normalized to data POT and is sorted into various truth topologies.

on D'Agostini's method with the MC truth as the prior [25]. The purpose of unfolding is to remove detector reconstruction related imperfections to achieve a more accurate representation of how the muon emerged from the interaction. By correcting the data samples from PØD water-in and water-out configurations separately, a subtraction procedure ultimately gives a cross section on water. Additionally, the MC is tuned to account for flux, interaction modeling, and detector corrections. The final tuned MC is then used to calculate efficiency corrections, purity corrections, and the unfolding matrix.

TABLE II. Number of water-out data events contained in the selected signal and sideband samples after each selection cut is applied. The cut on the number of Michel electrons is only applied to the CC1π^+ sample.

	Water-out data		
	Number of selected events		
Cut	CC0π	CC1π^+	CC Other
Data quality and PØD + TPC			
μ^- candidate in fiducial volume	33 083	33 083	33 083
Number of PØD tracks	13 370	8107	11 606
Number of Michel e^-	NA	1710	NA

TABLE III. Number of water-in data events contained in the selected signal and sideband samples after each selection cut is applied. The cut on the number of Michel electrons is only applied to the CC1π^+ sample.

	Water-in data		
	Number of selected events		
Cut	CC0π	CC1π^+	CC Other
Data quality and PØD + TPC			
μ^- candidate in fiducial volume	27 713	27 713	27 713
Number of PØD tracks	12 777	6297	8639
Number of Michel e^-	NA	1434	NA

The exclusive CC0π signal is evaluated by correcting the data selection based on the CC0π signal purity in the MC. The signal purity is calculated using the MC truth information and the data from the sideband samples. As described above, CC1π^+ interactions are the largest sources of background, followed by CCOther interactions. Therefore, sideband samples for these two backgrounds were selected as a data-driven background constraint. The ratio of the overall data sideband normalization to the overall MC sideband normalization is calculated and used to constrain the corresponding background in the CC0π MC selection as

$$B'_j = B_j \frac{S_d}{S_m}, \tag{1}$$

where j denotes a bin index, B' the sideband constrained background, B the original background in the MC signal selection, and S_d and S_m the sideband normalizations from data and MC respectively. This affects the signal purity used in the background correction,

$$p'_j = 1 - \frac{B'_j}{N'_{m,j}}, \tag{2}$$

where $N'_{m,j} = N_{m,j} - B_j + B'_j$ and N_m is the original number of events in the CC0π MC selection.

For this analysis, the initial prior used in the D'Agostini unfolding technique was taken from the MC truth and a single iteration is used. Fake-data studies showed that multiple iterations did not improve results but increased uncertainties. This increase is due to the correlation introduced between the data and successive priors [26] and can produce large fluctuations between neighboring bins. Additionally while in fake-data tests the total χ^2 for the unfolded result was slightly larger than expected ($\sim$1.7 not including any systematics), it did not significantly decrease with additional iterations. Thus a single iteration was chosen. This must be regarded as a regularized result. With the MC truth as the prior, a single iteration Bayesian unfolding matrix is equivalent to directly constructing an unfolding matrix based on the MC. This means that the unfolding matrix is calculated based on the mapping between truth and reconstructed kinematics in the MC.

To extract the neutrino cross section on water an additional subtraction step after the unfolding is required. The PØD fiducial volume contains plastic scintillator layers and thin brass sheets sandwiched between layers of water [16]. The water layers act as a passive target making it difficult to know whether an interaction occurred on water or on some other target nucleus. To work around this, the PØD was designed to be drained and filled during different run

periods. Everything being equal except for the inclusion or exclusion of water, a subtraction of the true water-in and water-out distributions should give the number of interactions on water. Since the PØD is in two different detector configurations with and without water, it is necessary to correct for detector smearing and inefficiencies before the subtraction. A direct subtraction of the reconstructed event rates would give an incorrect estimate for the actual event rate on water. Therefore, we first unfold the reconstructed distribution for water-in and water-out separately to get an approximation of their true distributions, then subtract the unfolded distributions to get the distribution of interactions on water. Specifically, this is given by

$$N_i^{\mathrm{H_2O}} = \frac{U_{ij}^w N_j^w}{\epsilon_i^w} - R\frac{U_{ij}^a N_j^a}{\epsilon_i^a}, \tag{3}$$

where the indexes i and j indicate true and reconstructed bins respectively, w and a indicate water-in and water-out periods respectively, N is the number of purity-corrected, signal events measured in the data signal selection, ϵ the selection efficiency, and R the flux normalization factor between water-in and water-out periods. U_{ij} represents the unfolding matrix. From this, the differential cross section on water can be expressed as

$$\frac{d\sigma}{dx_i} = \frac{N_i^{\mathrm{H_2O}}}{F^w N_n \Delta x_i}, \tag{4}$$

where F^w is the integrated flux over the water-in period, N_n the number of neutrons, and Δx_i the area of bin i across the phase space x. F^w is the POT-weighted flux of all water-in periods and calculated using flux simulations and from the constraints described above. As the water-in and water-out periods have different beam exposures, total flux for the water-out periods, F^a, is used to scale the flux normalization ratio, $R = F^w/F^a$. Additionally, correlated errors between the water-in and water-out periods are taken into account in the error propagation and discussed in Sec. III C.

C. Systematic uncertainties

As in previous T2K analyses, the systematic uncertainties can be separated into three principal categories: flux uncertainties, cross section model uncertainties, and detector uncertainties [9,27].

The flux and cross section errors are calculated by reweighting the individual simulated events. Once the events are reweighted, the unfolding matrix is regenerated and the cross section is recalculated using the new weights. The uncertainties for flux and cross section parameters are taken from the same covariance matrices used as inputs to the near detector fit in the T2K oscillation analysis [27]. There are 46 total parameters in the covariance matrix: 25 for flux, 6 for final-state interactions, and 15 other cross section parameters. By generating many throws for the model parameters and calculating the resulting event weights, we can calculate a covariance matrix for the final result. If $\frac{d\sigma_O}{dx_{i;k}}$ gives the cross section result for bin i and parameter throw k which has n throws, then the covariance between bins i and j is

$$\mathrm{cov}(i,j) = \frac{1}{n}\sum_{k=0}^{n-1}\left(\frac{d\sigma_O}{dx_{i;k}} - \frac{d\bar{\sigma}_O}{dx_i}\right)\left(\frac{d\sigma_O}{dx_{j;k}} - \frac{d\bar{\sigma}_O}{dx_j}\right) \tag{5}$$

where

$$\frac{d\bar{\sigma}_O}{dx_i} = \frac{1}{n}\sum_{k=0}^{n-1}\frac{d\sigma_O}{dx_{i;k}}. \tag{6}$$

The flux uncertainty is dominated by the uncertainty in the total flux normalization and is found to be 8.76%. Flux uncertainties are due in large part to uncertainties in the hadron production model but are affected by beam line uncertainties as well [15]. A parametrization in neutrino energy and flavor is used to propagate flux uncertainties. Cross section model uncertainties include both uncertainties in basic neutrino-nucleus scattering and uncertainties from FSI [27]. Parameters that govern the neutrino interaction and nuclear description models used in the NEUT generator [21] are used to propagate cross section uncertainties.

Neutrino-nucleus scattering depends on nucleon form factors and the nuclear medium model. Neutrino generators typically assume a dipole form factor governed by an axial mass parameter for QE and resonant charged-current interactions. Additionally, many of the interaction parameters tune the normalization on certain interaction channels that are poorly understood. These include 2p2h contributions that arise from multinucleon correlations inside the nucleus. The current understanding of these multinucleon interactions is based on the meson exchange model where two nucleons exchange a meson current such that the charged-current interaction involves both nucleons. This is expected to enhance the CCQE-like cross section. Thus, instead of a single final state nucleon, two or more nucleons may be ejected out of the nucleus. Other parameters, such as the nuclear binding energy and the Fermi momentum describe the nuclear medium.

An intranuclear cascade model describes secondary pion propagation within the nucleus [28]. Uncertainties on FSI are calculated by tuning the pion production, absorption, rescattering and charge-exchange probabilities.

The primary neutrino generator used for this analysis is a tuned version of NEUT 5.3.2 [21,29]. The tuning is applied based on best-fit values from a fit of three models implemented in NEUT to external MINERνA and MiniBooNE CCQE measurements [30]. The NEUT model uses the Smith-Moniz relativistic Fermi gas model [31] with a relativistic random phase approximation (RPA) [32]

TABLE IV. The fractional uncertainties on the restricted phase space cross section due to several of the individual cross section parameters.

Source	Uncertainty [%] on cross section
M_A^{QE}	0.8
M_A^{RES}	0.3
CA5 single-pion interaction	0.5
2p2h normalization (^{16}O)	2.8
E_b (^{16}O)	0.05
p_F (^{16}O)	0.2

and a multinucleon exchange (2p2h) model [32,33]. An axial mass of $M_A^{\mathrm{QE}} = (1.15 \pm 0.03)$ GeV/c^2, the amplitude of the multinucleon effects 2p2h norm $= (27 \pm 12)\%$, and Fermi momentum $p_F = (223 \pm 5)$ MeV/c were used. The uncertainties in these parameters are propagated to the final cross section measurement. A secondary neutrino generator used for testing is GENIE 2.8.0 [34].

Table IV shows the individual contributions of several interaction model parameters to the total cross section. Note that the 2p2h normalization, binding energy E_b, and Fermi momentum p_F are nuclei dependent. These are calculated with 100 throws without taking correlations into account. This illustrates and identifies the effects of a single parameter on the cross section result. For the final result, 800 throws were used along with covariances across the full parameter-space to generate the interaction and other systematic uncertainties, and 2000 throws were used for statistical errors. The lower number of throws used in Table IV means there is a larger statistical error on the uncertainty itself.

Detector systematics describe uncertainties in reconstructed properties of events rather than the underlying physics. These are separated into weight systematics and variation systematics. Weight systematics modify the weight to be applied to simulated events. These include effects such as differences in tracking efficiencies between data and simulation. Variation systematics modify observables such as the reconstructed particle momentum of a simulated event. These allow for migration of events between different kinematic bins. Systematics related to the uncertainty on the fiducial mass must be treated in a different manner, as these affect both the expected number of events and the total mass used to normalize the cross section measurement.

The event reconstruction in the PØD uses a Kalman filter algorithm to calculate the properties of tracks found in the detector. The reconstructed momentum will primarily be influenced by two main effects: the curvature of the track in the tracker and the energy loss within the PØD. Because relatively little information about the track curvature can be obtained by the PØD and because the small amount of energy loss in the tracker will have little effect on the reconstructed initial momentum, the systematics for these two effects are treated separately. Uncertainties in the energy loss in the PØD are estimated from a sample of cosmic ray muons that pass through the tracker and stop in the PØD. To propagate these uncertainties, the reconstructed momentum in the simulation is altered by

$$(\Delta p)^{\mathrm{P\O D}}_{\mathrm{scale}} = (x_s \sigma_s)(p^{\mathrm{reco}} - p^{\mathrm{reco}}_{TPC1}) \tag{7}$$

for the scale uncertainty and

$$(\Delta p)^{\mathrm{P\O D}}_{\mathrm{res}} = (x_r \sigma_r)(p^{\mathrm{reco}} - p^{\mathrm{reco}}_{TPC1} - p^{\mathrm{truth}} + p^{\mathrm{truth}}_{TPC1}) \tag{8}$$

for the resolution uncertainty. In these equations σ represents the uncertainty and x is a normally distributed random number that changes for each systematics throw. Similar numbers are obtained for both the water-out and water-in geometries, and a 1.4% uncertainty is applied to the energy loss scale and a 7% uncertainty to the resolution. Tracker curvature systematics follow the same procedure as for previous T2K analyses [27]. Scale and resolution uncertainties are applied to the momentum extrapolated from the track curvature. Additional uncertainties are applied to account for distortions in the magnetic field, charge misidentification, TPC cluster reconstruction, and TPC track reconstruction. Studies have shown that the PØD track reconstruction and matching PØD tracks to TPC tracks have an efficiency greater than 99.8%, so no correction or uncertainty is applied due to this.

In some cases, an interaction that occurred outside the fiducial volume will be reconstructed in the fiducial volume. Using the nominal NEUT simulation, such out of fiducial volume events represent 2.89% of events in the water-in sample and 3.95% of events in the water-out sample. An analysis of the spatial distribution of events in the layers of the PØD central electromagnetic calorimeter, immediately downstream of the water target, suggests that there may be as much as a factor of 2 discrepancy in the amount of migration between data and simulation (but this is a small fraction of the total number of events). To account for this, we increase the weights of events originating in the central electromagnetic calorimeter by a factor of 2 and add an uncertainty of 50% of the initial weight. The distributions of these events in the two PØD geometries are identical, as there is no water in these layers. These events will cancel out up to small differences in statistics and the detector response, so a large uncertainty corresponds to a small effect on the final result. The detector systematics are summarized in Table V

The one-track selection is sensitive to pileup where particles from several interactions are reconstructed in the PØD in the same bunch. The main pileup sources are cosmic ray muons, multiple neutrino interactions in the same beam bunch, and interactions occurring in the material outside ND280 (called sand events) that produce

TABLE V. Detector systematic uncertainties considered in this analysis. The uncertainty in each category gives the overall uncertainty on the restricted phase space cross section, calculated for 100 throws. The final result in Eq. (9) throws all uncertainties simultaneously and uses a larger number of throws.

Systematic	Uncertainty [%]
PØD energy loss scale	1.3
PØD energy loss resolution	6.7
Tracker momentum scale	1.5
Tracker momentum resolution	0.2
Magnetic field distortion	0.04
Charge ID efficiency	0.1
TPC cluster efficiency	0.3
TPC track efficiency	0.4
Out of fiducial volume	0.8
Detector mass	1.5

tracks in the PØD. The cosmic ray muon pileup rate is estimated to be approximately 2×10^{-4} per bunch, which is negligible. The beam-related pileup rate is dominated by sand events, and is calculated separately for each ND280 run period. The sand muon corrections are given in Table VI.

Finally, there is some uncertainty in the total target mass. Mass uncertainties change the total number of events expected as well as the total number of target nuclei used to obtain the correct cross section normalization. Because the PØD is composed of several materials, the mass uncertainty also has a small effect on the smearing matrix, since the cross section shape will not necessarily have the exact same shape for different materials. In the case of the water in the fiducial volume, the total mass of the water is known very well, but there is still uncertainty in how the water is distributed throughout the different layers. Measurements have shown that there is approximately 15% more water in the most downstream water layer compared to more centrally located layers. There is also a smaller uncertainty on the amount of water in individual layers away from the edges. To estimate the uncertainty due to the mass, a 0.8% uncertainty on the total water mass is applied with additional 15% uncertainties in the layers at the ends of the water target and 5% uncertainties on the remaining layers. The layer-by-layer variations are performed keeping the total mass fixed. These give us an uncertainty of 1.5% due to the target mass.

TABLE VI. Sand event pileup rates for each ND280 run period. The weights of simulated events are reduced by a factor of $1 - p_{\text{sand}}$.

Run	p_{sand} [bunch^{-1}]
2 water	0.0144
2 air	0.0173
3c	0.0188
4 water	0.0217
4 air	0.0245

For all systematic errors, correlations between the water-in and water-out periods were taken into consideration in Eq. (3). This was done by ensuring identical seeding for throws in calculating Eq. (5). Since flux uncertainties do not distinguish between water-in and water-out samples the flux uncertainties should be fully correlated. The oxygen binding energy parameter affects only the water-in sample, which means that the overall cross section uncertainties are not fully correlated. Some PØD-specific detector systematics, such as the PØD target mass systematic, have dependence on the water state. Thus detector systematics are not fully correlated either. Further, any differences between water-in and water-out detectors are taken into account with different standard deviations on the underlying variations. Statistical errors are treated as uncorrelated.

IV. RESULTS

The result shown in Fig. 6 uses data from T2K Runs 2–4. It is reported as a double differential cross section in the outgoing muon kinematics $(p_\mu, \cos\theta_\mu)$. Black data points taken from Eq. (4) show the double differential result with full error bars. The colored error bars show the cumulative uncertainties from various sources, starting with the data statistics and ending with the detector systematics. Errors from each source are added in quadrature. MC predictions from NEUT 5.3.2 (tuned) and GENIE 2.8.0 are shown as solid and dashed blue lines.

The fractional contribution from each source of uncertainty is shown in Fig. 7, binned and plotted in the same scheme as Fig. 6. In most regions, the statistical error from the data is the single most dominant source of bin-by-bin uncertainty, but overall the statistical errors are comparable to the total systematic uncertainty. Aside from the low sensitivity bins, the fractional bin-by-bin errors lie on the order of 10%–20%.

This result is compared to the T2K CC0π cross section on C_8H_8 [9] in Fig. 8. Since both results were obtained using the T2K flux, the error bars shown do not include the flux uncertainty. The binnings do not exactly match between the two analyses, but when overlaid, both results appear to be consistent within uncertainties for most of the phase space. The largest areas of discrepancy are in the high-angle regions, where the CC0π water cross section is higher than the hydrocarbon cross section.

Finally, the result is compared to the Martini *et al.* [35] model predictions on carbon in Fig. 9 and the SuSAv2 model predictions on water [36,37] in Fig. 10. Both models are shown with and without 2p2h. Overall, our result agrees better with an inclusion of 2p2h in most regions of phase space. This is consistent with a similar comparison performed for the measurement on C_8H_8 [9].

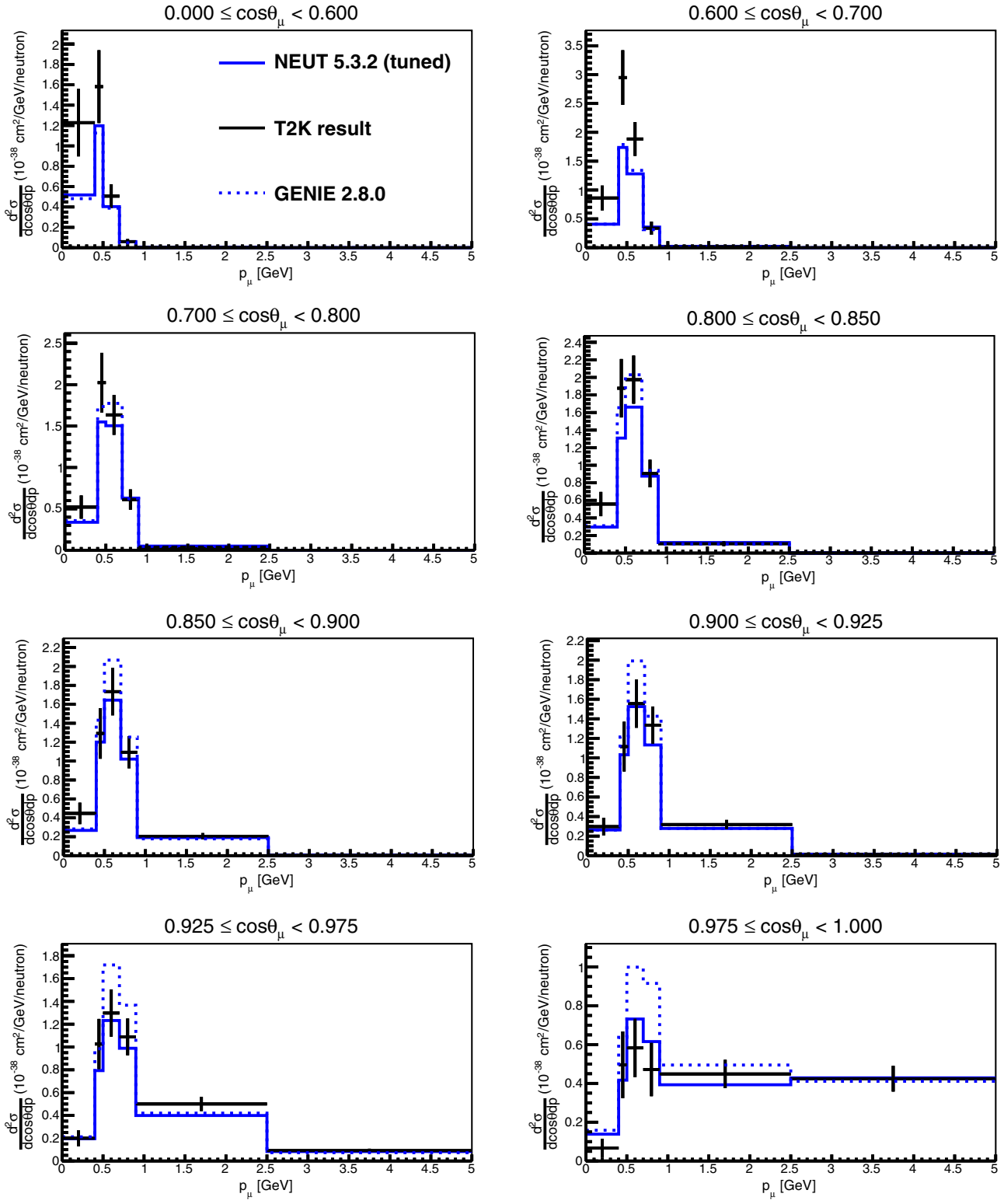

FIG. 6. The double differential ν_μ CC0π cross section on water for each slice in $\cos\theta_\mu$.

The unfolding procedure allows events to migrate into and out of regions in the phase space outside the binned area. Specifically, this "out-of-range" region refers to where $\cos\theta_\mu < 0$ or $p_\mu > 5$ GeV. As the selection efficiency here is very low, we calculated a reduced, total cross section by integrating over only to the explicitly binned areas of the $(p_\mu, \cos\theta_\mu)$ phase space. The reduced, total cross section was found to be

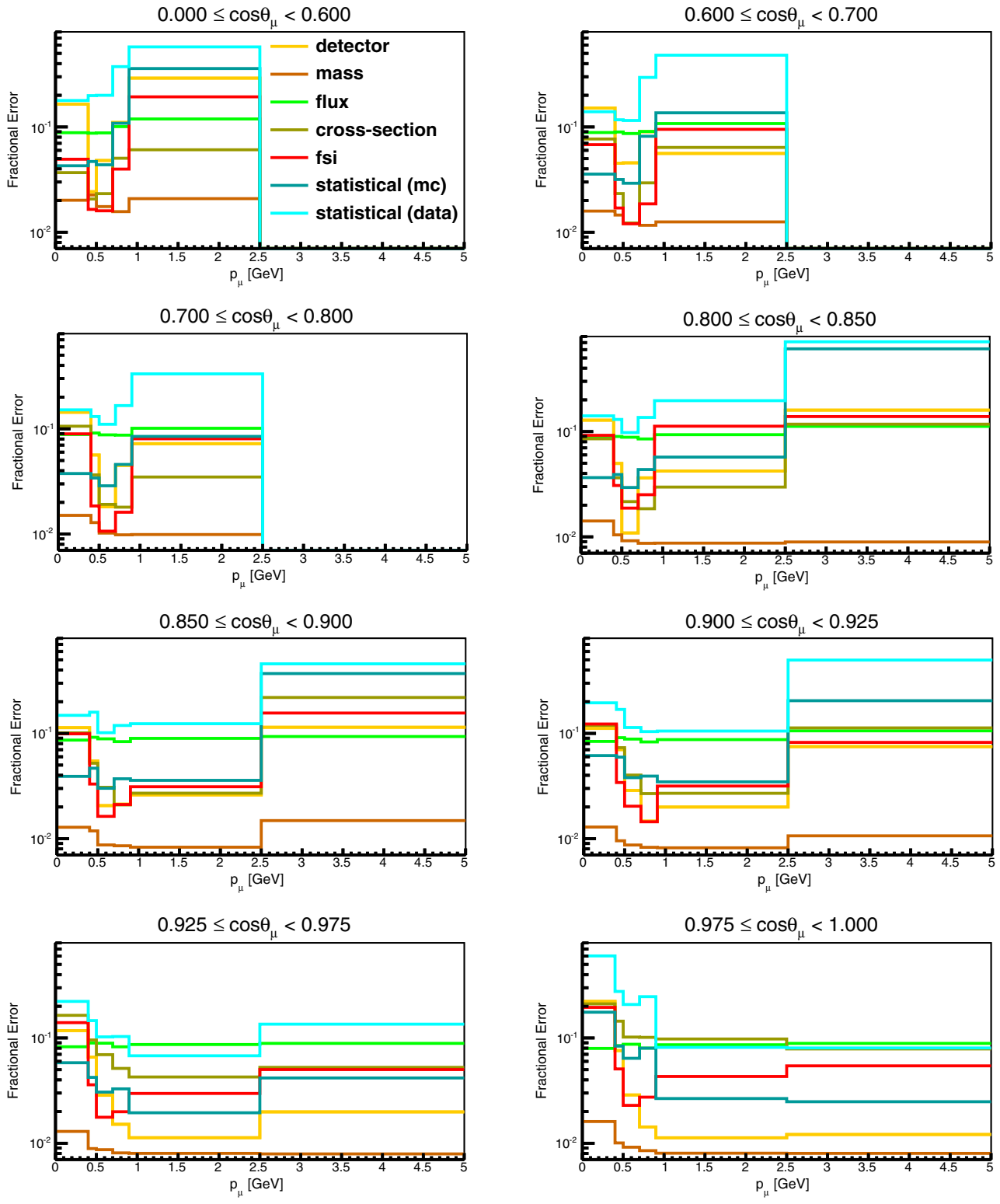

FIG. 7. The fractional error from each source of uncertainty on the double differential ν_μ CC0π cross section on water.

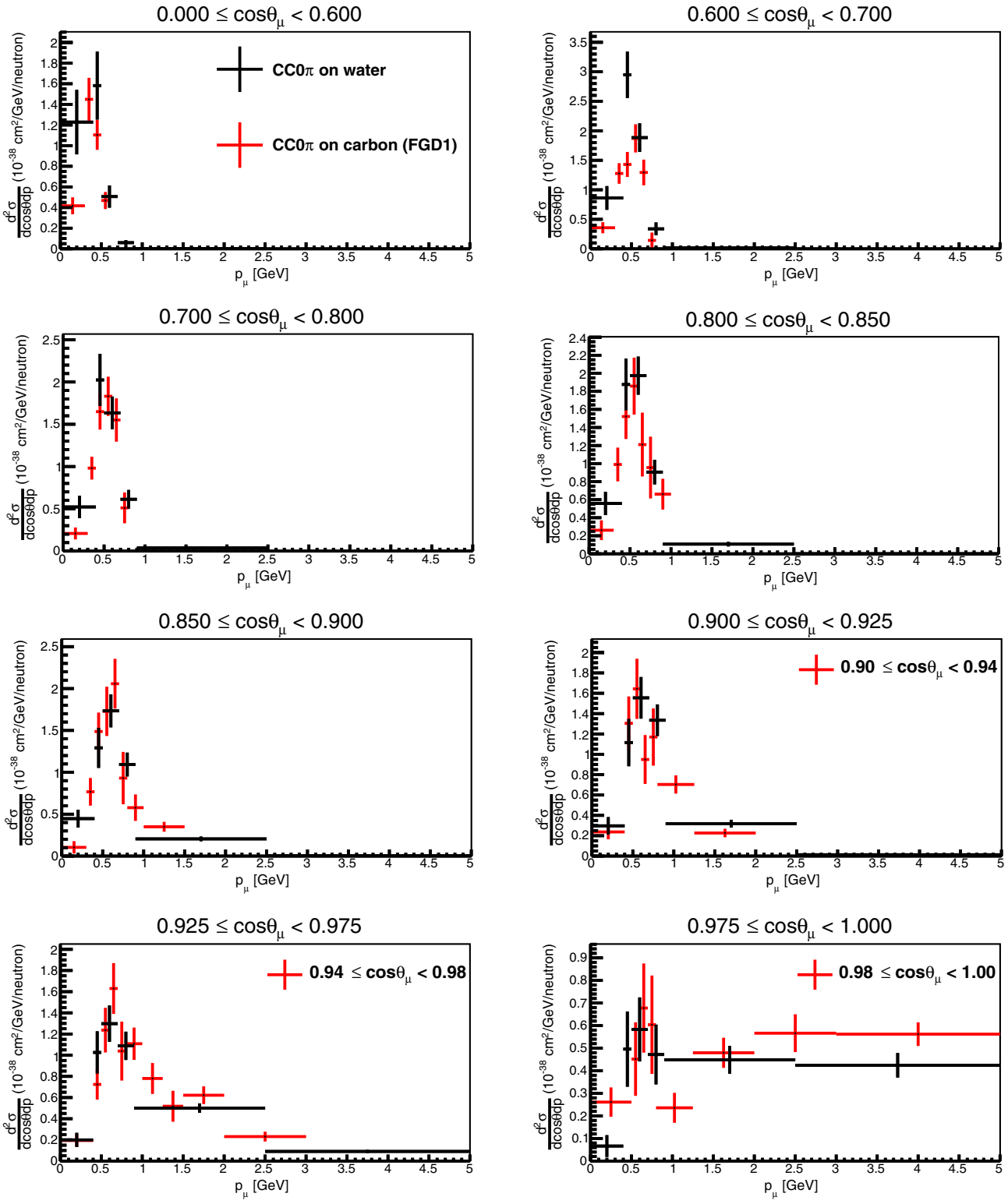

FIG. 8. Here, the CC0π water cross section from the PØD is overlaid with the CC0π C_8H_8 cross section previously measured by T2K [9]. The error bars shown include all sources of uncertainty *except* the flux. In regions where $\cos\theta_\mu$ slices are different between the water and hydrocarbon result, the bin edges are noted in the legend.

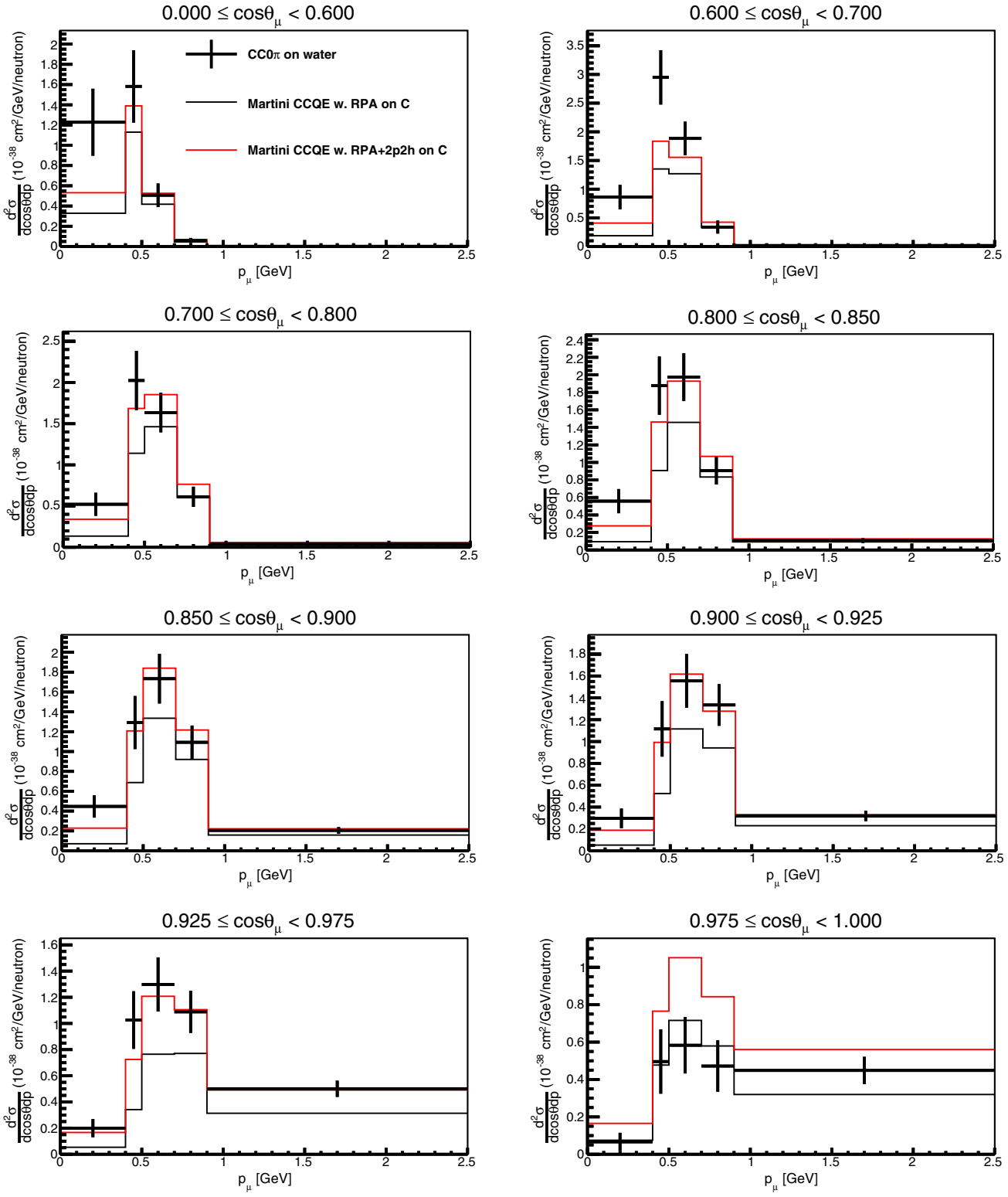

FIG. 9. A comparison of the CC0π water cross section against two Martini model predictions on carbon, one with 2p2h contributions and one without.

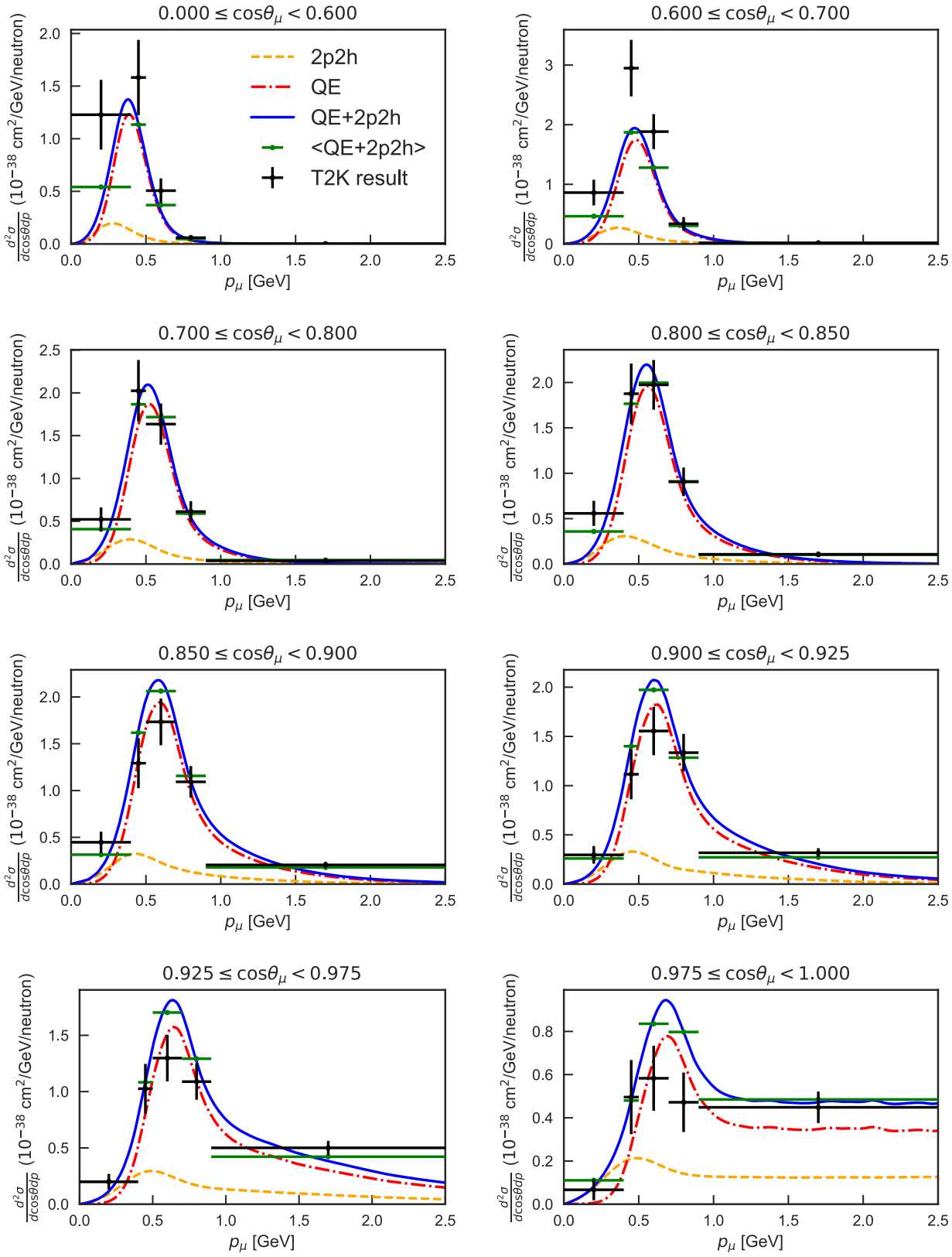

FIG. 10. A comparison of the CC0π water cross section against the SuSAv2 model. Predictions for CCQE and 2p2h on oxygen are shown separately along with their sums and average over the bins.

TABLE VII. Fractional uncertainties on the total cross section.

Source	Uncertainty [%]
Statistics (data)	7.7
Statistics (MC)	1.8
Detector mass	1.5
Detector other	6.3
FSI	3.4
Cross section	3.2
Flux	8.7

$$\sigma^{\mathrm{CC0}\pi}_{\nu_\mu \mathrm{H_2O}} = 0.95 \pm 0.08(\mathrm{stat}) \pm 0.06(\mathrm{det\ syst}) \pm 0.04(\mathrm{model\ syst}) \pm 0.08(\mathrm{flux}) \times 10^{-38}\ \mathrm{cm}^2/\mathrm{n}. \quad (9)$$

This is significantly higher than the NEUT (GENIE) prediction of $0.66(0.68) \times 10^{-38}$ cm^2/n primarily due to the disagreement between data and MC in the high-angle regions, which cover a large portion of the reduced phase space. The breakdown of the fractional uncertainties on Eq. (9) are given in Table VII.

V. CONCLUSION

Using the T2K near detector, ND280, a CCQE-like, flux-integrated cross section on water was reported here in the double-differential phase space of the outgoing muon. Since the $\bar{\nu}_\mu$ contribution to this sample is insignificant, this is effectively a measurement on oxygen. The result complements previous T2K cross section measurements. A comparison to a double-differential cross section result on carbon [9] shows good agreement with the exception of a few low momentum bins in the high-angle region. Comparisons were also performed to T2K simulations using NEUT [21] and GENIE [34]. Overall it appears that the tuned NEUT prediction is favored over GENIE, but in the angular regions of $0.7 < \cos\theta_\mu < 0.85$ it shows better agreement with GENIE. Another comparison to the Martini *et al.* [35] CCQE prediction with and without 2p2h prefers the 2p2h contribution. A comparison to the SuSAv2 model predictions [36,37] also generally agrees with the data within errors, though the data points tend to be lower than the model in the more forward regions.

New techniques for CCQE measurements, such as exploring the transverse kinematics space, or incorporating proton kinematics are ongoing in T2K. Future analyses from T2K will have the benefit of higher statistics and can also include antineutrino cross sections.

The fluxes used for this result, the extracted cross section values and covariance matrices for the errors are available at [38].

ACKNOWLEDGMENTS

We thank the J-PARC staff for superb accelerator performance. We thank the CERN NA61/SHINE Collaboration for providing valuable particle production data. We acknowledge the support of MEXT, Japan; NSERC (Grant No. SAPPJ-2014-00031), NRC and CFI, Canada; CEA and CNRS/IN2P3, France; DFG, Germany; INFN, Italy; National Science Centre (NCN) and Ministry of Science and Higher Education, Poland; RSF, RFBR, and MES, Russia; MINECO and ERDF funds, Spain; SNSF and SERI, Switzerland; STFC, UK; and DOE, USA. We also thank CERN for the UA1/NOMAD magnet, DESY for the HERA-B magnet mover system, NII for SINET4, the WestGrid and SciNet consortia in Compute Canada, and GridPP in the United Kingdom. In addition, participation of individual researchers and institutions has been further supported by funds from ERC (FP7), H2020 Grant No. RISE-GA644294-JENNIFER, EU; JSPS, Japan; Royal Society, UK; the Alfred P. Sloan Foundation and the DOE Early Career program, USA.

[1] K. Abe *et al.* (T2K Collaboration), Nucl. Instrum. Methods Phys. Res., Sect. A **659**, 106 (2011).
[2] K. Abe *et al.* (T2K Collaboration), Phys. Rev. D **85**, 031103 (2012).
[3] K. Abe *et al.* (T2K Collaboration), Phys. Rev. Lett. **112**, 061802 (2014).
[4] Y. Fukuda *et al.* (Super-Kamiokande Collaboration), Nucl. Instrum. Methods Phys. Res., Sect. A **501**, 418 (2003).
[5] K. Abe *et al.* (T2K Collaboration), Phys. Rev. Lett. **112**, 061802 (2014).
[6] A. A. Aguilar-Arevalo *et al.* (MiniBooNE Collaboration), Phys. Rev. D **81**, 092005 (2010).
[7] J. L. Alcaraz-Aunion and J. Walding (SciBooNE Collaboration), AIP Conf. Proc. **1189**, 145 (2009).
[8] G. A. Fiorentini *et al.* (MINERvA Collaboration), Phys. Rev. Lett. **111**, 022502 (2013).
[9] K. Abe *et al.* (T2K Collaboration), Phys. Rev. D **93**, 112012 (2016).
[10] K. Abe *et al.* (T2K Collaboration), Phys. Rev. D **92**, 112003 (2015).
[11] R. Gran *et al.* (K2K Collaboration), Phys. Rev. D **74**, 052002 (2006).
[12] T. Sekiguchi *et al.* (T2K Collaboration), Nucl. Instrum. Methods Phys. Res., Sect. A **789**, 57 (2015).

[13] N. Abgrall *et al.* (NA61/SHINE Collaboration), Eur. Phys. J. C **76**, 84 (2016).
[14] N. Abgrall *et al.* (NA61/SHINE Collaboration), J. Instrum. **9**, P06005 (2014).
[15] K. Abe, N. Abgrall, H. Aihara *et al.* (T2K Collaboration), Phys. Rev. D **87**, 012001 (2013).
[16] S. Assylbekov *et al.* (T2K ND280 PØD Collaboration), Nucl. Instrum. Methods Phys. Res., Sect. A **686**, 48 (2012).
[17] N. Abgrall *et al.* (T2K ND280 TPC Collaboration), Nucl. Instrum. Methods Phys. Res., Sect. A **637**, 25 (2011).
[18] P. A. Amaudruz *et al.* (T2K ND280 FGD Collaboration), Nucl. Instrum. Methods Phys. Res., Sect. A **696**, 1 (2012).
[19] D. Allan *et al.* (T2K ND280 ECAL Collaboration), J. Instrum. **8**, P10019 (2013).
[20] S. Aoki *et al.*, Nucl. Instrum. Methods Phys. Res., Sect. A **698**, 135 (2013).
[21] Y. Hayato, Nucl. Phys. B, Proc. Suppl. **112**, 171 (2002).
[22] S. Agostinelli *et al.* (GEANT4 Collaborations), Nucl. Instrum. Methods Phys. Res., Sect. A **506**, 250 (2003).
[23] J. Allison *et al.*, IEEE Trans. Nucl. Sci. **53**, 270 (2006).
[24] J. A. Formaggio and G. P. Zeller, Rev. Mod. Phys. **84**, 1307 (2012).
[25] G. D'Agostini, Nucl. Instrum. Methods Phys. Res., Sect. A **362**, 487 (1995).
[26] T. Adye, arXiv:1105.1160.
[27] K. Abe *et al.* (T2K Collaboration), Phys. Rev. D **91**, 072010 (2015).
[28] L. Salcedo, E. Oset, M. Vicente-Vacas, and C. Garcia-Recio, Nucl. Phys. **A484**, 557 (1988).
[29] Y. Hayato, Acta Phys. Pol. B **40**, 2477 (2009).
[30] C. Wilkinson *et al.*, Phys. Rev. D **93**, 072010 (2016).
[31] R. A. Smith and E. J. Moniz, Nucl. Phys. **B43**, 605 (1972); **B101**, 547(E) (1975).
[32] J. Nieves, I. R. Simo, and M. J. Vicente Vacas, Phys. Rev. C **83**, 045501 (2011).
[33] R. Gran, J. Nieves, F. Sanchez, and M. J. Vicente Vacas, Phys. Rev. D **88**, 113007 (2013).
[34] C. Andreopoulos, C. Barry, S. Dytman, H. Gallagher, T. Golan, R. Hatcher, G. Perdue, and J. Yarba, arXiv:1510.05494.
[35] M. Martini, M. Ericson, G. Chanfray, and J. Marteau, Phys. Rev. C **80**, 065501 (2009).
[36] J. E. Amaro, M. B. Barbaro, J. A. Caballero, T. W. Donnelly, A. Molinari, and I. Sick, Phys. Rev. C **71**, 015501 (2005).
[37] G. D. Megias, J. E. Amaro, M. B. Barbaro, J. A. Caballero, and T. W. Donnelly, Phys. Rev. D **94**, 013012 (2016).
[38] http://t2k-experiment.org/wp-content/uploads/nd280data-numu-cc0pi-xs-on-h2o-2017.tar.gz.